



Alkene epoxidation with mesoporous materials assembled from TS-1 seeds – Is there a hierarchical pore system?

Markus Reichinger^b, Wolfgang Schmidt^c, Maurits W.E. van den Berg^a, Alexander Aerts^d, Johan A. Martens^d, Christine E.A. Kirschhock^d, Hermann Gies^b, Wolfgang Grünert^{a,*}

^a Lehrstuhl für Technische Chemie, Ruhr-Universität Bochum, Bochum, Germany

^b Institut für Geologie, Mineralogie und Geophysik, Ruhr-Universität Bochum, Bochum, Germany

^c Max-Planck-Institut für Kohlenforschung, Mülheim/Ruhr, Germany

^d Centrum voor Oppervlaktechemie en Catalyse, KU Leuven, Leuven, Belgium

ARTICLE INFO

Article history:

Received 1 October 2009

Revised 21 November 2009

Accepted 23 November 2009

Available online 12 January 2010

Keywords:

Hierarchical pore systems

Zeolite seeds

TS-1

Epoxidation

XANES

ABSTRACT

Hexagonal mesoporous solids were synthesized from solutions containing TS-1 seeds. The products were characterized by XRD, nitrogen and argon physisorption, TEM, TG/DTA of template decomposition (also after extraction of the mesopore template), UV-Vis and IR spectroscopy, and XANES at the TiK edge. Their catalytic activities were assessed for cyclohexene epoxidation in hydrophilic and hydrophobic environment (CH₃OH/water, with H₂O₂ oxidant, and decane, with *tert*-butyl hydro-peroxide oxidant, respectively) and for *n*-hexene epoxidation in hydrophilic environment. The mesopore system was clearly documented by XRD, physisorption measurements, and TEM, whereas evidence for micropores by physisorption proved elusive. However, the micropore template was detected in the solids by TG/DTA even after extraction of the mesopore template, and among the Ti sites, which were confirmed to be tetrahedrally coordinated by UV-Vis and XANES, a clear majority was able to coordinate two water molecules. It was concluded that the pore walls had been built up from nanoparticulate TS-1 precursors resulting in walls of ca. 1.5 nm thickness, which resemble rather the exterior layers of a TS-1 crystallite than its (hydrophobic) interior. In cyclohexene epoxidation, the micro-mesophases were by 1–2 orders of magnitude more active than TS-1 and outperformed also Ti-MCM-41, at similar selectivity in hydrophobic medium. With 1-hexene in hydrophilic medium, however, the micro-mesophases failed completely whereas TS-1 exhibited high activity.

© 2009 Elsevier Inc. All rights reserved.

1. Introduction

The synthesis of solids with hierarchical pore systems [1,2] is a promising field of present research in catalysis. Microporous materials provide unique catalytic functions, for example, strong zeolitic acidity and highly selective use of peroxo oxygen by framework Ti, but present considerable diffusional barriers, in particular, for liquid reactants. There are several approaches to alleviate this situation. Mesoporosity has been created in zeolite crystals, e.g., by zeolite synthesis around mesopore templates such as carbon particles [3] and polymers [4], or by desilication causing partial dissolution of the framework [5,6]. The use of zeolite nanocrystals [7], the partial recrystallization of mesoporous silicas into zeolite phases [8], the direct synthesis of zeolites in the presence of organosilane mesopore templates [9], and the synthesis of ordered mesoporous materials

(OMMs) from zeolite seeds [10–12] are alternative routes. The latter approach appears highly appealing because it combines a mesopore surface area of many hundreds of m²/g with regions of zeolite-like connectivity, too small to be detected by X-ray diffraction.

Various groups have described the synthesis of micro-meso OMMs (mostly hexagonal phases) with seeds of different zeolites – ZSM-5 [13,14], Y [10], Beta [11,13], but also TS-1 [12,15–19]. In all cases, the formation of mesopore systems is beyond any doubt, but characterization of the microporous part is a challenge. Any crystalline domain large enough to allow resolution by XRD would just demonstrate the failure of the synthesis, and adsorption models fail describing short micropore segments in contact with a mesopore system. However, microporosity can be traced by analysis of the local environment of framework elements and micropore templates. In the case of aluminosilicate seeds, a variety of methods are available: ²⁷Al-NMR, acidity measurements, and test reactions for acidic sites all probe the properties imparted by the heteroatom. IR spectroscopy can give clues on the overall framework connectivity, manifesting in characteristic zeolite framework vibrations, like the band at 550 cm⁻¹ considered as a fingerprint for the pentasil

* Corresponding author. Address: Lehrstuhl für Technische Chemie, Ruhr-Universität Bochum, P.O. Box 102148, D-44780 Bochum, Germany. Fax: +49 234 32 14115.

E-mail address: w.gruenert@techem.rub.de (W. Grünert).

[20]. For the NMR inactive titanium in titanosilicate building blocks, the choice of characterization techniques is more limited. The presence of TS-1-like structures has been largely judged by UV–Vis spectroscopy, which can prove the tetrahedral coordination of the Ti, but not its complete accessibility, and by its IR fingerprint (framework band at 960 cm^{-1}). The latter is, however, overshadowed in materials where a large abundance of silanol groups is to be expected [21]. In addition, the reactivity in test reactions has been used as an additional support for the success of the preparations, which is unfortunately rather ambiguous as the same reactions can also be catalyzed by Ti in fully disordered titania silicate walls. Recently, ^{129}Xe NMR has been utilized to examine the presence of micropores in micro-meso OMM materials, and while the data clearly suggested differences between the micro-meso preparations and a reference material with amorphous pore walls, the signal indicating microporosity was very weak, much broader than in TS-1 and appeared only at very low temperatures [22].

We present here the results of an attempt to characterize the microporosity in hexagonal **micro-meso** OMMs with **1-dimensional hexagonal mesopore system** made from **TS-1** seeds (“mime-1h(TS-1)”) in detail, giving full account on a project, whereof preliminary data have been reported previously in Ref. [23]. Methods employed beyond those used in the earlier literature on micro-meso OMMs are the selective decomposition of micro and mesopore templates, Ar physisorption, and TiK XANES. It could be demonstrated that all the Ti sites are tetrahedrally coordinated and almost completely accessible from the gas phase, however, the typical TS-1 signature of 0.5–0.6 nm micropores was not detected in pore-size distributions derived from Ar physisorption data. This was ascribed to the small size of the seeds of only 1.5–2 nm used to form the mesopore walls, possibly preventing the typical capillary phenomena by the small length of the micropore. Interestingly, the catalysts exhibited the expected catalytic properties (large superiority over TS-1 and Ti-MCM-41) in the epoxidation of cyclohexene but failed completely when oxidation of *n*-hexene was attempted.

2. Experimental

2.1. Synthesis of micro-meso OMMs

Micro-meso OMMs were synthesized from a liquid containing TS-1 seeds. For the preparation of these seeds, 35.9 mmole of tetraethyl orthosilicate (TEOS, Aldrich, 98% GC) was added dropwise and under vigorous stirring to an aqueous solution of tetrapropyl ammonium hydroxide (TPAOH, BASF, alkali free; a 40 wt.% solution containing 6.4 mmole). After 30 more minutes of stirring, 0.55 mmole of tetra-*n*-butyl orthotitanate (TBOT, Merck), and, after a 10 min mixing period, 340 mmole of water were added dropwise during continuous agitation. The resulting zeolite precursor solution with a molar ratio TEOS:TPAOH:TBOT:H₂O of 1:0.35:0.02:15.45 was aged at 293 K for 24 h. From this precursor solution, a conventional TS-1 could be obtained by heating in an autoclave at 433 K for 10 d, with the resulting XRD and IR characteristics close to the industrial reference TS-1 sample mentioned below [24].

Mime-1h(TS-1) was obtained from this seed mixture by adding 16.5 mmole of cetyltrimethylammoniumbromide (CTAB, Aldrich, as a 10 wt% aqueous solution at 353 K) after 20 min of continuous stirring at room temperature. This procedure is known to yield mesophases with hexagonally ordered unimodal parallel pores with a number of different framework sources. The solid product was then recovered by filtration, washed several times with distilled water, and dried at 333 K for 24 h. Most of the material prepared was subjected to a hydrothermal treatment the effect of which has been described in detail in [24]. For this purpose, as-syn-

thesized micro-meso material was mixed with distilled water and held in an autoclave at 413 K for one day. The products obtained will be labeled as “ht”. They were recovered by filtration and further washed and dried as already described. The templates were removed in a stepwise procedure. CTAB was extracted by refluxing the samples three times in an ethanolic acetic acid solution for 1 h (twice with 0.2 vol.% acetic acid for 1 h, once with 0.1 vol.% acetic acid, with intermediate washing in ethanol). The product was then again dried at 333 K for 24 h. The remaining TPAOH was removed by oxidation first at 573 K and then at 723 K for 1 h, with a heating rate of 1 K/min from room temperature to final temperature.

Mime-1h(TS-1) was prepared in three batches under identical conditions, and the data for two of these are reported to demonstrate the reproducibility of the synthesis. These batches will be differentiated by the subscripts “a” and “b”. The data for the third batch were comparable as far as measured.

An analogous cubic micro-meso OMM was also obtained from the TS-1 seed mixture, and some characterization and reactivity data of this material are reported in [23,24]. As the characterization of this material has remained incomplete by now, we will focus here on the hexagonal OMM materials.

For comparison, characterization and catalytic studies were also performed with an industrial TS-1 and a conventional Ti-MCM-41 prepared according to Corma et al. [25].

2.2. Characterization

Sample compositions were determined by ICP-OES after dissolution along the sodium perborate route. Measurements were made with a Philips PU 7000 ICP Spectrometer.

Powder XRD was performed with a Philips diffractometer (flat plate sample holder, Bragg-Bretano geometry) using Cu K α radiation. Measurements with long exposure were made with an Image Plate Guinier Camera (Huber) with Cu K α_1 radiation and a germanium monochromator. The samples were kept in glass capillaries of 0.3 mm diameter.

Transmission IR spectra were recorded with a Perkin Elmer 882 spectrometer, with the samples diluted with KBr (1:500) before pressing them into self-supported wafers.

Nitrogen physisorption data were obtained with a Nova 4200e instrument (Quantachrome) after degassing the samples in vacuum for 2 h at 673 K. Argon physisorption was measured on an ASAP 2010 instrument (Micromeritics) after degassing at 350 °C in vacuum for 3 h. All physisorption data were processed with the non-local density functional theory (NLDFT) algorithm of the NovaWin software package (Quantachrome) using the respective kernels based on equilibrium adsorption in cylindrical pores in silica.

TEM images were obtained with a JEOL-2000FX instrument applying an acceleration voltage of 200 kV. UV–Vis spectra were measured in diffuse reflection on a Lambda 9 spectrometer (Perkin Elmer).

Temperature-programed decomposition of the templates employed to generate the porous solids can be used to differentiate the meso and micropore systems, provided the templates differ in decomposition temperatures. By comparing the data of a sample containing all templates with the results obtained after CTAB extraction (*vide supra*), it should be possible to detect if the TPAOH was indeed retained in micropores and not simply dissolved in the CTAB phase. CTAB extraction was performed as described above. DTA and TG were performed with an STA 503 instrument (Bähr, 3 K/min temperature ramp in air from 298 K to 1073 K).

XANES spectra of the Ti K-edge at 4966.0 eV were measured in transmission mode at Hasylab E4 station (Hamburg) using a Si(1 1 1) double crystal monochromator. Powder samples were diluted in BN and pressed into a wafer, which was mounted in an

in situ cell [26]. The spectra were taken in the as-received state and after dehydration, which was achieved by heating in flowing helium at 573 K (10 K/min temperature ramp) for 30 min. In case of TS-1, dehydration was performed at 673 K. The spectra were taken at room temperature, the spectra of a Ti foil was recorded at the same time (between the second and third ionization chambers) for energy calibration. Data treatment was carried out using the software package VIPER [27]. The spectra were normalized based on the edge jump.

2.3. Catalysis

The catalytic reactivity of the micro-mesophases was tested for the epoxidation of cyclohexene and of 1-hexene. These reactions were performed in hydrophilic medium (methanol/water) with an inorganic oxidant (H_2O_2) and in hydrophobic medium (decane) with an organic peroxide (*tert*-butyl hydroperoxide, TBHP). The reactions were performed in batch regime as follows: hydrophilic medium – 0.9 M cyclohexene (or 1-hexene) in CH_3OH , 0.45 M H_2O_2 (35% aqueous solution), 0.03 g catalyst, at 313 K for 24 h, hydrophobic medium – 0.9 M cyclohexene in decane, 0.45 M TBHP (in decane), 0.03 g catalyst, at 313 K for 24 h. Analysis and identification were carried out with GC–MS.

3. Results

In Table 1, the samples prepared in this study and the reference materials are listed, their Si/Ti ratios and BET surface areas are

given, and the labels used for them throughout the paper are introduced. No BET surface areas are given for TS-1 as the BET equation does not apply for micropore systems.

Low-angle X-ray diffractograms of the mime-1h(TS-1) materials are shown in Fig. 1, where the states after synthesis and after the hydrothermal treatment (with templates in the pores) are compared with the final evacuated states. Without hydrothermal treatment, the resulting diffraction lines are rather broad, and the (1 1 0) and (2 0 0) reflections are not resolved. These clearly emerge after the hydrothermal treatment, which apparently increases the order in the material considerably. The hydrothermal treatment also leads to a significant extension of the pore system (cf. lattice parameters collected in Table 1). This has also been observed with purely siliceous micro-meso OMMs [24] and is known for OMMs with amorphous walls [28]. Irrespective of hydrothermal treatment of the materials, template removal by calcination shifts the reflections to slightly larger angles indicating smaller unit cells. This effect is known from OMMs with amorphous walls where it has been ascribed to the densification of the walls due to ongoing condensation reactions. The two batches compared in Fig. 1 are rather similar although mime-1h(TS-1)_a seems to be less ordered after calcination without hydrothermal treatment. After the hydrothermal procedure, however, both batches are well ordered.

A wide-angle X-ray diffractogram of mime-1h(TS-1)_a is shown in Fig. 2, and the region where the most intense reflections of TS-1 are expected is enlarged in the inset. It is obvious that the material does not contain Bragg crystalline phases such as TiO_2 and TS-1

Table 1
Titania silicate materials used in the present study.

Sample ^a	Si/Ti	BET surface area ^b (m ² /g)	Lattice parameter a_0 (nm)	Av. pore diameter (nm) (NLDFT)
Mime-1h(TS-1) _a	56	n.d.	3.93	–
Mime-1h(TS-1) _a -ht	52	949	5.24	4.25
Mime-1h(TS-1) _b	62	1215	4.02	3.25
Mime-1h(TS-1) _b -ht	70	990	5.27	4.25

^a Reference materials: Ti-MCM-41 – Si/Ti = 35; TS-1 – Si/Ti = 33.

^b N₂ physisorption at 77 K.

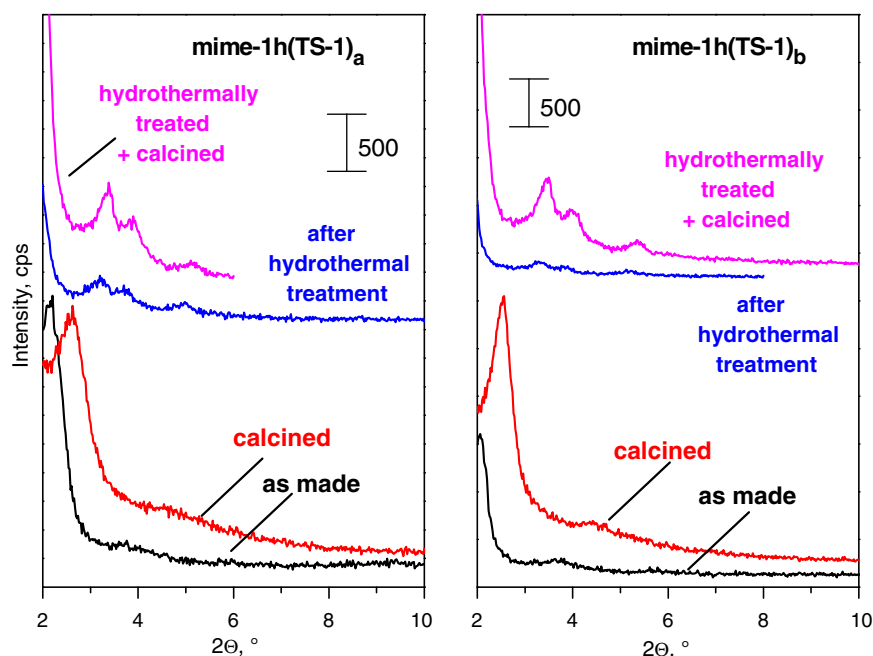


Fig. 1. Small-angle X-ray diffractograms of mime-1h(TS-1)_a and mime-1h(TS-1)_b – with and without hydrothermal treatment, before and after template removal.

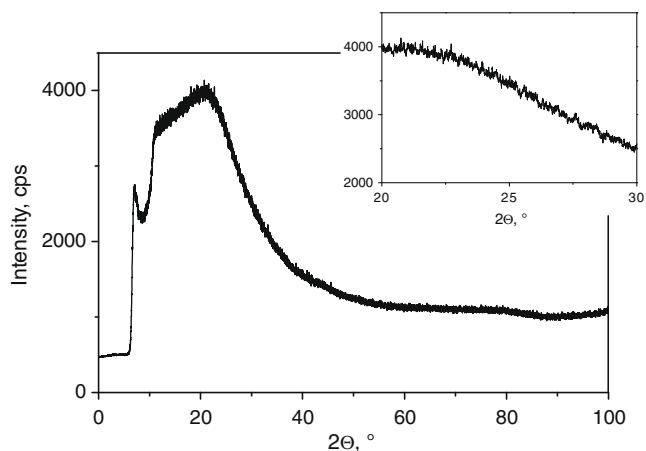


Fig. 2. Wide-angle X-ray diffractogram of mime-1h(TS-1)_a. Typical range of TS-1 reflections zoomed in inset.

that would give rise to Bragg reflection. This holds also for the other micro-meso materials listed in Table 1.

In the IR wavelength region typical of zeolite lattice vibrations, all samples exhibited a distinct band located at 562–567 cm^{-1} , i.e., significantly higher than the 550 cm^{-1} band taken as the MFI fingerprint. The spectra are reported in [24].

In Fig. 3a, the N_2 and Ar physisorption isotherms of mime-1h(TS-1)_b-ht are compared. The pore-size distributions (PSDs) are given in Fig. 3b (nitrogen, incl. mime-1h(TS-1)_a-ht, gray stars) and 3c (Ar). As expected from XRD, the mesopores become larger and the PSD becomes narrower after the hydrothermal treatment. The nitrogen-based PSD of mime-1h(TS-1)_a-ht is similar to that of the companion sample, with somewhat more pronounced tailing toward larger sizes [24]. The average mesopore sizes, which are recorded in Table 1, are between 3.2 and 4.2 nm.

From the Ar-based PSD of mime-1h(TS-1)_b-ht (Fig. 3c), disappointingly little evidence for microporosity can be derived. The

micropore volume was just 0.005 cm^3/g , out of a total pore volume of 0.73 cm^3/g (with nitrogen, a larger total pore volume of 0.95 cm^3/g was obtained). In particular, no peak in the 0.5–0.6 nm range, which would be expected for TS-1, can be observed. The micropores seem to be largely represented by a weak tailing of the PSD down to 1.5 nm including a small hump at 1.6 nm. Ar physisorption on a third companion sample (cf. 2.1.) resulted in a similar PSD though with an additional very small peak at 0.8 nm. The micropore volume of this material was of the same order as that of mime-1h(TS-1)_b-ht. Geometric models with the lattice parameters and pore diameters as given in Table 1 allow the estimations of specific surface areas for OMMs with amorphous walls, e.g., MCM-41. Assuming a specific density of the walls of 2.0 g/cm^3 (specific densities of 1.9–2.1 g/cm^3 have been measured for various silica OMMs in our laboratories), geometric surface areas are ob-

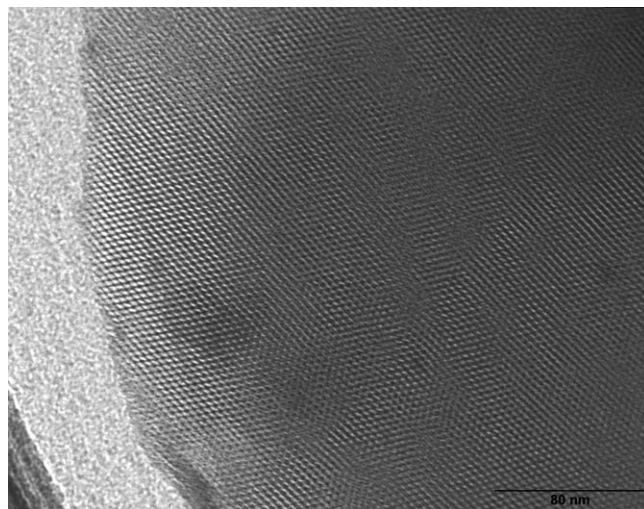


Fig. 4. TEM micrograph of mime-1h(TS-1)_b-ht.

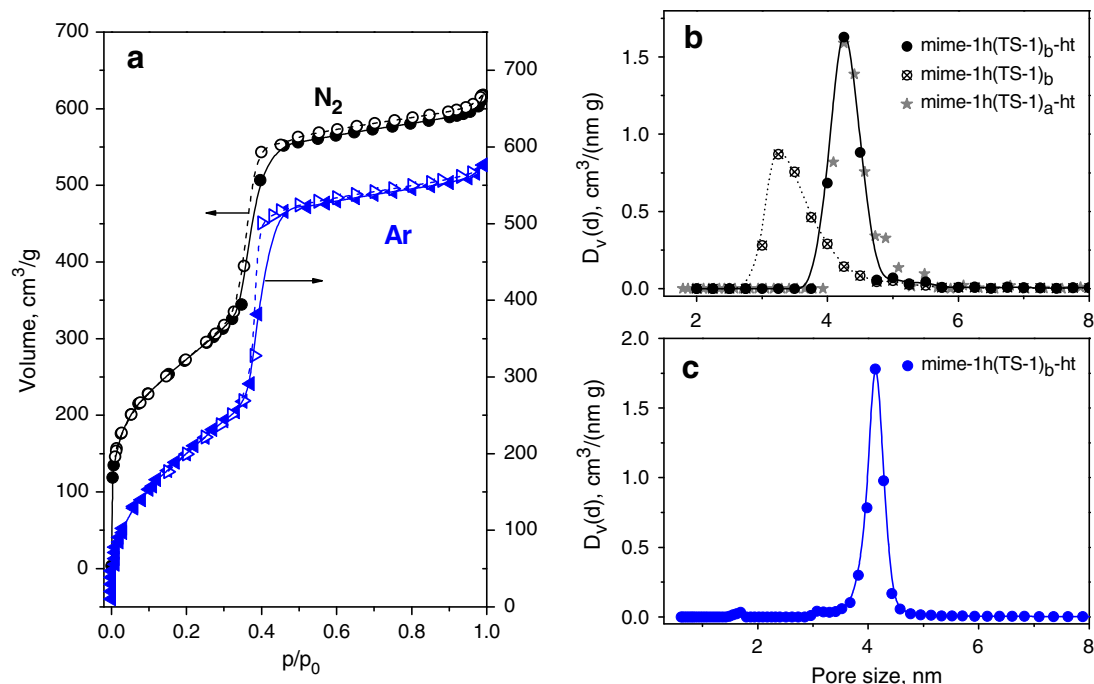


Fig. 3. Physiosorption studies of micro-mesophases from TS-1 seeds. (a) Adsorption isotherms for N_2 (77 K) and Ar (87 K) for mime-1h(TS-1)_b-ht, (b) N_2 -derived pore-size distributions, and (c) Ar-derived pore-size distribution of mime-1h(TS-1)_b-ht.

tained which are about 250–300 m²/g lower than those measured on our individual samples. This indicates substantial surface roughness of the pore walls which might be caused by micropore openings of nanoscopic MFI fragments.

A TEM image of mime-1h(TS-1)_b-ht is given in Fig. 4. It shows a very regular hexagonal array of pores with low defect density. The periodicity extends to the rim of the particle in this material. Such quality was not always achieved, because amorphous surface layers (at excellent periodicity beneath) were seen in the third companion batch mentioned in Section 2.1 [24]. The quality of the image in Fig. 4 permits the estimation of the wall thickness after further magnification. According to this, the walls are no more than 1.5 nm thick, i.e., their dimensions are in the order of the unit cell dimensions of TS-1 and comparable to the original size of the used TS-1 seeds.

The differentiation of micropore and mesopore templates by thermal analysis is exemplified in Fig. 5 with the results for mime-1h(TS-1)_b. Fig. 5a shows the TG and DTA curves of the as-made material, the same experiment after extraction of CTAB (cf. Section 2.2.) is depicted in Fig. 5b. The weight losses in Fig. 5a can be attributed to the removal of residual water (low temperatures), to the decomposition of CTAB starting around 430 K, to the decomposition of TPA-OH starting around 570 K, and the condensation of the silicate structure, which becomes prominent at higher temperatures. These events appeared in the same temperature regions in many other purely siliceous or Ti-containing micro-meso OMMs, and the assignments were supported by template decomposition studies with known pore systems [24]. After CTAB extraction, the sample loses much less weight than before (Fig. 5b). The weight loss around 570 K now accounts for most of the total weight loss. Apparently, CTAB was successfully extracted from the mesopores, but TPA-OH was retained. This TPA-OH would have been extracted if it had been dissolved in the CTAB filling the micropores or if it had been only physisorbed on the walls' surface. Therefore, the experiment qualitatively supports the presence of micropores reminiscent of the MFI structure type in the sample.

UV-Vis spectroscopy and XANES have been used to characterize the coordination of the Ti species. Many groups have used UV-Vis spectroscopy to characterize micro-meso materials containing TS-1 structural motives, and their spectra mostly consist of a broad band centered at 210–220 nm [19,29] or even up to 230 nm [18]. The spectra of TS-1 and of our mime-1h(TS-1) preparations are reported in Fig. 6. There is no significant difference between these spectra, they all consist of a broad band peaking at 200–210 nm, i.e., the coordination of the Ti atoms in the micro-meso materials is very similar compared to TS-1. Only in one case (mime-1h(TS-

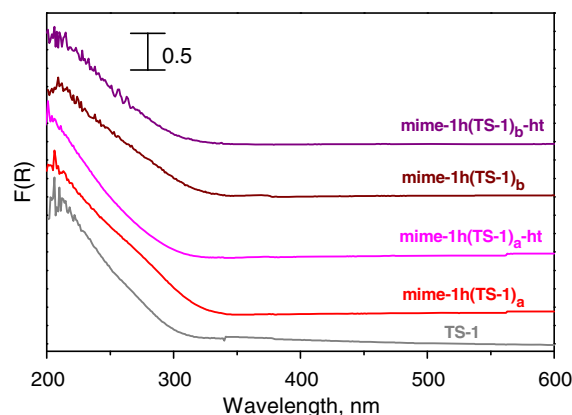


Fig. 6. UV-Vis spectra of micro-mesophases from TS-1 seeds and of crystalline TS-1 (reference).

1)_a), there is a minor shoulder above 250 nm where signals are usually assigned to isolated Ti in higher coordinations [30].

XANES at the TiK edge has been widely used to establish coordination geometries of first-row transition metal species. A pre-edge 1s–3d transition, which is forbidden in ligand fields with inversion symmetry but can achieve considerable intensity in tetrahedral geometry, is used for this purpose. In contrast to UV-Vis spectroscopy where adsorbates such as H₂O and NH₃ in the Ti coordination sphere cause only minor shifts of the absorption band, the XANES pre-edge peak for TS-1 is highly sensitive to coordination geometry [31]. The XANES spectra of dehydrated mime-1h(TS-1) batches and of reference compounds are compared in Fig. 7a. In Fig. 7b and c, the effect of dehydration is demonstrated for TS-1 and for mime-1h(TS-1)_b-ht. Signal positions and heights (relative to the step height) are summarized in Table 2. It can be seen that the pre-edge peak, indicating tetrahedral Ti coordination, is well developed in all studied micro-meso samples. However, this holds only after dehydration: after storage in atmosphere, the pre-edge peak of our micro-mesophases is much smaller and shifted to higher energies by 0.5–0.8 eV. Opposed to this, the pre-edge peak in TS-1 is almost unaffected after storage in air. The latter seems to be a peculiarity of the used industrial material. Usually significantly larger attenuations of this peak by interaction with H₂O were reported in the literature [31].

The catalytic results are summarized in Tables 3 and 4. In Table 3, the data for cyclohexene oxidation in hydrophilic medium

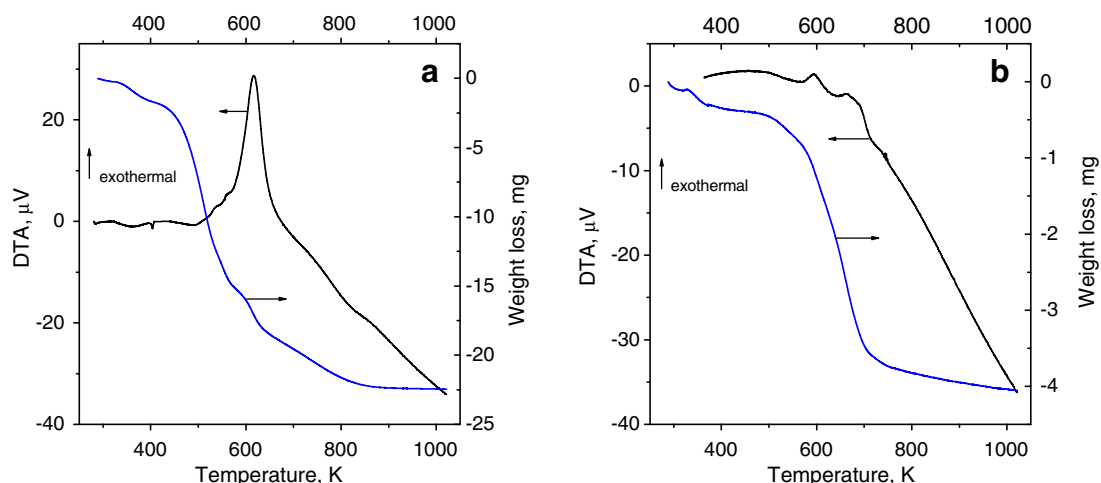


Fig. 5. Thermal analysis (DTA – left scale, TG – right scale) of mime-1h(TS-1)_b. (a) As made, containing both templates – CTAB and TPA-OH, and (b) after extraction of CTAB.

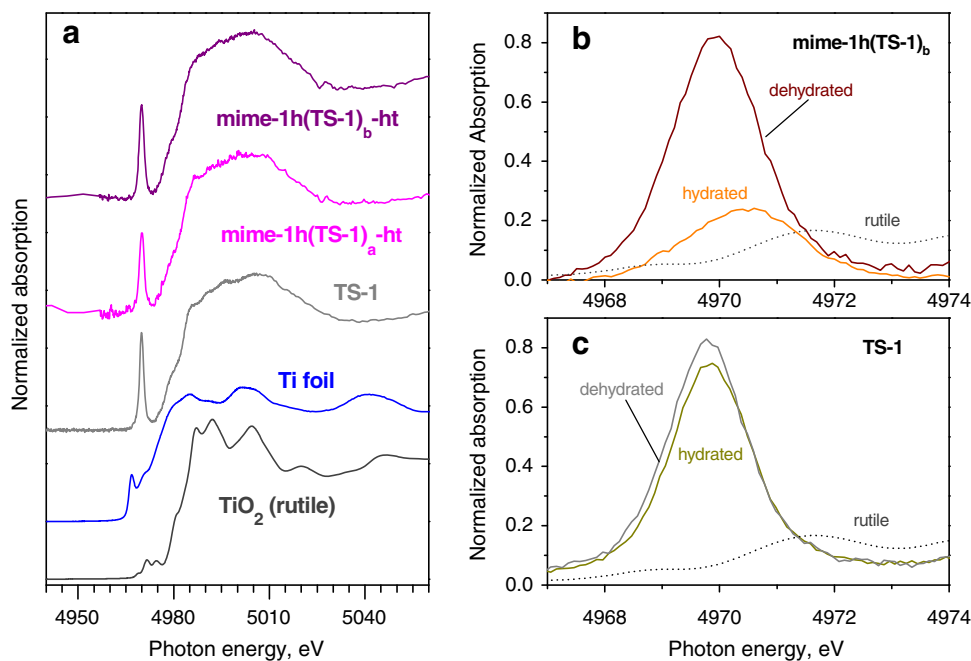


Fig. 7. X-ray absorption study of micro-mesophases from TS-1 seeds. (a) TiK XANES spectra of mime-1h(TS-1) preparations after hydrothermal treatment (dehydrated state), comparison with reference compounds, (b) influence of hydration on the pre-edge peak of mime-1h(TS-1)_b, and (c) influence of hydration on the pre-edge peak of TS-1.

Table 2
XANES parameters of mime-1h(TS-1) samples compared with TS-1.

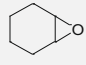
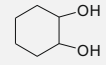
Sample	State	E^a (eV)	Relative height ^b
TS-1	Stored in air	4969.8	0.74
	Dehydrated	4969.8	0.83
Mime-1h(TS-1) _a	Stored in air	4970.1	0.35
	Dehydrated	n.d.	n.d.
Mime-1h(TS-1) _a -ht	Stored in air	4970.6	0.22
	Dehydrated	4970.0	0.69
Mime-1h(TS-1) _b	Stored in air	4970.6	0.24
	Dehydrated	4969.9	0.82
Mime-1h(TS-1) _b -ht	Stored in air	4970.5	0.26
	Dehydrated	4969.9	0.80

^a Position of pre-edge peak.

^b Height of pre-edge peak relative to step height.

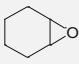
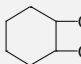
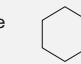
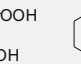
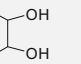
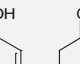
are given. Despite the lower Ti content, the cyclohexene conversions were greatly increased with the micro-meso materials compared to Ti-MCM-41 or even TS-1. There were, however, variations in selectivity, although these have to be treated with great caution due to the large differences in conversion. The most important feature is the extent of epoxidation and allylic oxidation which are known to be competing reactions, i.e., their ratio should not depend very strongly on conversion. The epoxide is not stable in this environment and is easily converted with water or methanol into cyclohexanediol or methoxy cyclohexanol. The micro-meso mate-

Table 4
Cyclohexene epoxidation with TBHP.

Catalyst	X (%)	S (%)		
				Unknown
Mime-1h(TS-1) _a	35	92	4	2/2
Mime-1h(TS-1) _a -ht	35	86	6	4/4
Ti-MCM-41	5.7	95	5	–
TS-1	0.3	95	5	–

rials appear to have a somewhat lower epoxidation selectivity than Ti-MCM-41 (and, probably, TS-1) and, correspondingly, a larger tendency to catalyze allylic oxidation. Allylic oxidation products are formed through a hydroperoxide intermediate. Interestingly, instead of cyclohexane diol a hydroperoxide ring-opening product of the epoxide could be traced in the products obtained with the micro-mesophases, but not with Ti-MCM-41 or TS-1 (cf. Table 3). The hydroperoxide character of this product was proven by its ability to oxidize trimethylphosphine to triphenylphosphine oxide. The formation of this hydroperoxide adduct may indicate a larger concentration of the hydroperoxide in the reaction mixture of the micro-meso catalysts and may explain the larger selectivity for allylic oxidation.

Table 3
Cyclohexene epoxidation with H₂O₂.

Catalyst	X (%)	S (%)						Epoxide derivatives (%)	Allylic products (%)
									
Mime-1h(TS-1) _a	47	<1%	35	4	–	35	26	39	61
Mime-1h(TS-1) _a -ht	47	<1%	42	2	–	32	24	44	56
Ti-MCM-41	25	2	31	–	24	18	24	58	42
TS-1	4	6	13	–	57	11	11	70	22

A very surprising result was obtained when 1-hexene was substituted for cyclohexene in the catalytic runs. With 1-hexene, the micro-meso phases did not give any conversion. This is very remarkable given their large activity with respect to cyclohexene. TS-1 yielded 33% hexene conversion under these conditions, with a selectivity of 88% for epoxide and products derived thereof.

The results for cyclohexene epoxidation in hydrophobic medium (i.e., with TBHP) are summarized in Table 4. Here, the micro-mesophases show the expected advantage over TS-1: the conversions are by two orders of magnitude larger, at almost equal selectivity. Under these conditions, allylic oxidation does not take place at all. Surprisingly, a minor quantity of hydrolysis product was found. With the cubic product reported in [23,24] (according to our labeling mime-3c(TS-1)), an epoxide selectivity of 95% was indeed achieved though at a slightly lower conversion of 26%. With the micro-mesophases, some additional reaction products were observed in minor amounts, which could not yet be identified (presumably TBHP adducts). These were not found in the reaction mixtures of Ti-MCM-41 and TS-1. 1-Hexene conversion in hydrophobic medium was 1% with TS-1, this reaction was therefore not attempted with the micro-mesophases.

The catalytic properties of the micro-mesophases are remarkable although only the structurally less perfect mime-1h(TS-1)_a and its hydrothermally treated version were studied. There was however no significant difference between these two materials, which suggests that structural perfection of the mesopore system might have no critical influence on the catalytic activity.

4. Discussion

Most of the data presented above complies with the general situation met in many studies on mesophases synthesized from zeolite seeds: dimension and order of the mesopore system are more readily documented than the microporosity of the material. Here too, XRD and physisorption measurements (Figs. 1 and 3) together with TEM analysis (Fig. 4) indicate highly ordered hexagonal mesopore systems. A successful incorporation of Ti into the mesophase is suggested by wide angle-XRD (Fig. 2) where Bragg crystalline Ti-containing phases (e.g., TS-1, TiO₂) were not detected. The UV-Vis spectra (Fig. 6) are similar to those of TS-1 and show the tetrahedral coordination of Ti in the solid. This is supported by the XANES data (Fig. 7, Table 2) where the intensity of the pre-edge peak at the TiK edge agrees with that found in TS-1. However, all this is not sufficient to decide if the wall structure is fully amorphous or ordered and porous. The Ar physisorption results seem to exclude the presence of zeolite-like microporosity, as no PSD maximum typical of MFI pore sizes was observed.

A first indication for the presence of zeolite-like connectivity in the sample is the observation of a signal in the region of the MFI IR fingerprint, though at somewhat higher wave numbers. It is well known that this band can also arise from other pentasil structures built from five-membered rings (FER, MOR) but is absent in amorphous silica [32]. The wave number of this band has been shown experimentally [33] and by theoretical molecular dynamics simulations [32] to depend on the size and degree of condensation of the pentasil fragment. The increased wave numbers therefore confirm the expectation that the materials contain structure motifs reminiscent of the MFI topology in building blocks of the size of the original TS-1 seeds.

The XANES data of the hydrated samples are of some relevance for the puzzle as well. After storage in ambient atmosphere, the pre-edge peak at the TiK edge is somewhat smaller but hardly shifted in crystalline TS-1, but much smaller and significantly shifted to larger energies in all investigated mime-1h(TS-1) materials. According to an extensive study on the dependence of this

pre-edge peak on the Ti coordination geometry, Farges et al. [34] concluded that 4-, 5-, and 6-fold Ti coordination can be distinguished by combining the information from peak position and height (cf. Fig. 8). According to this, the Ti exists as a mixture of 4- and 6-coordinated species in mime-1h(TS-1)_b with and without hydrothermal treatment and in mime-1h(TS-1)_a-ht, while for mime-1h(TS-1)_a, the result is less clear. In this mixture, most sites are in 6-fold coordination (Fig. 8), which suggests that for most of the Ti sites in our samples, two vacancies are accessible from the gas phase. In fully amorphous walls a significant amount of Ti should be completely excluded from access by molecules in the mesopores.

The difference in the dehydration behavior of our micro-meso materials and of TS-1 is another interesting feature. The TS-1 studied by us was obviously very hydrophobic as expected for a crystal with few defects where hydrophilic properties are confined to the external surface region. Upon dehydration, there is no shift in the XANES pre-edge peak energy and hardly any decrease in peak height (cf. Table 4, Fig. 8). The TS-1 material studied by Bordiga et al. [35] showed a somewhat stronger effect, which is indicated by an arrow in Fig. 8: the peak was not shifted either, but it decreased by ca. 50%. Apparently, the hydrophilicity of the Ti in our samples is much larger compared to Ti in TS-1 crystals, and appears to resemble the behavior typical for Ti in the external surface regions of TS-1. This suggests that the locally ordered zeolite-like arrays are very small, i.e., there is not much interior zeolite-like volume where the hydrophobic properties of TS-1 could manifest.

Finally, the results of temperature-programed template decomposition also support the view that there is microporosity in our samples. Indeed, the decomposition of the mesopore and micropore templates (CTAB and TPA-OH, respectively) could be well distinguished by thermal analysis, in particular by TG. After extraction of the CTAB from the mesopores, TPA-OH remained in the sample, i.e., it was locked in the TS-1 seeds. One may therefore conclude that the tetrahedral, well accessible Ti sites were indeed part of a structure forming voids where the template resided after synthesis, although the size of these microporous domains is not large enough to develop the hydrophobic properties of TS-1 crystals.

As only the pore walls can host the deduced microporous structures, the wall thickness provides a limit for one of the dimensions

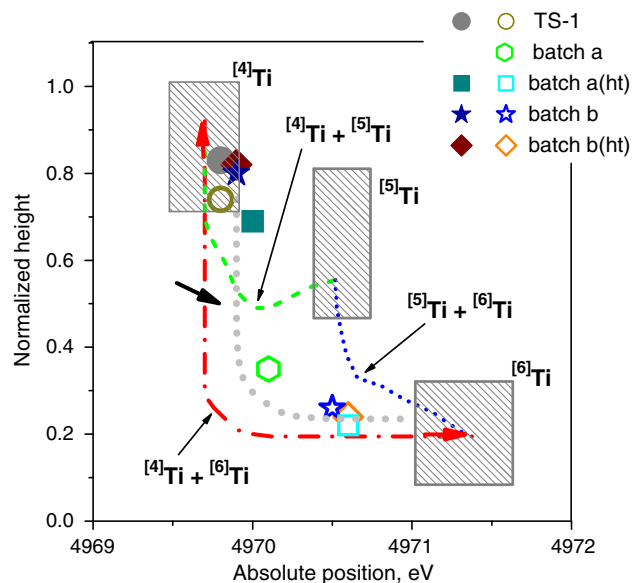


Fig. 8. Assessment of Ti coordination from the TiK XANES pre-edge peak according to Istitien (for numerical data see Table 2). Full signals - dehydrated state, open signals - hydrated state, for explanation of arrow see text.

of the microporous domains. From the TEM images, the wall thickness is in the order of 1.5 nm. The wall thickness may be also derived from the XRD and physisorption data as it is the difference between lattice parameter and pore diameter. All these data should be considered as a gross estimate because of considerable uncertainty, e.g., in porosity assessment and thickness determination from TEM images. From the physisorption and XRD data in Table 1, a wall thickness between 0.8 and 1.2 nm can be derived. This is certainly somewhat underestimated, but the agreement with the estimates from TEM is still remarkable. Hence, the wall thickness is probably not larger than 1.5–2 nm, which is also the maximally possible thickness of the microporous domains, except for the spandrel between three mesopores where it is presumably slightly thicker. Thus, the formation of our micro-mesophases appears to comply with the formation mechanism of mesophases (“zeolites”) from zeolite seeds put forward in [36,37]: the solid is probably formed from nanoparticulate TS-1 precursors with emerging TS-1 connectivity. Assembled by the mesostructuring agent, a wall thickness of 1.5 nm results.

On this basis, the puzzling failure of Ar physisorption to detect the micropores typical of the MFI structure becomes clear: there is porosity but no extended pores: In the very thin mesopore walls the voids originally formed by TPA cations in the nanoparticle precursors would not be experienced as “pores” by the adsorbate entering from *both* sides, but just as surface roughness which certainly yields no capillary phenomena comparable to extended ordered zeolite connectivity.

Both in hydrophobic and in hydrophilic media, our micro-mesophases from TS-1 seeds are more active than those from Ti-MCM-41 and TS-1 in the liquid-phase oxidation of cyclohexene with peroxy reagents. In hydrophilic environment, our materials seem to be less selective for epoxidation than TS-1, but a safe conclusion cannot be drawn as the data have been taken at different conversion levels. The vast superiority in activity over TS-1 may be ascribed to the excellent accessibility of the active sites for the cyclohexene molecule which has to diffuse through micropores in TS-1, but through mesopores in our mime-1h(TS-1) or mime-3c(TS-1) catalysts. The difference to Ti-MCM-41 may result from differences in accessibility and in coordination: in Ti-MCM-41, part of the Ti will be occluded in the amorphous walls, and usually only part of the Ti is in tetrahedral coordination in such materials. The probably larger selectivity of our micro-mesophases toward allylic oxidation is tentatively assigned to the abundance of surface OH groups, which should be similar in Ti-MCM-41 exhibiting similar selectivity properties. In hydrophobic environment, allylic oxidation is unimportant, and the advantage of the micro-mesophases, in particular over TS-1, is fully visible.

The complete failure of the same catalyst to oxidize *n*-hexene in hydrophilic medium is attributed to a combination of diffusional and interaction effects. In TS-1, *n*-hexene meets much lower diffusional resistance and is therefore much better converted than cyclohexene. Conversely, in the more hydrophilic environment originating from assembly of TS-1 precursors into micro-meso materials, the solvents compete favorably with this molecule which will not stay in the cavities for long once it enters them. This should be different with cyclohexene because of its larger size and a somewhat less pronounced hydrophobicity, thus conversion with the hydroperoxide can occur.

5. Conclusions

Solid catalysts with hexagonal mesopore systems were prepared from solutions containing TS-1 nanoparticulate precursors and characterized with respect to their structure and their catalytic behavior in epoxidation reactions. For the best-characterized hex-

agonal materials, the identity of the mesopore system could be clearly confirmed by XRD, TEM, nitrogen, and Ar physisorption. The IR signature of MFI frameworks was observed at somewhat increased wave numbers (562–567 cm⁻¹) in accordance with an expected very small size of the TS-1 building blocks. TG/DTA studies of template decomposition suggested that the micropore template remained in the solid after the mesopore template had been extracted. After removal of both templates, TiK XANES showed that the large majority of Ti sites, which were all tetrahedrally coordinated according to UV-Vis and XANES evidence, were able to coordinate two water molecules from the gas phase. N₂ physisorption provided physical surface areas significantly larger than expected if the pores were separated by dense walls. On this basis, the existence of a micropore system was concluded although the expected micropores were not evident in the pore size distributions from N₂ and Ar physisorption. This mismatch was ascribed to the extremely small dimensions of the microporous building units which form pore walls of <2 nm thickness. This small dimension would also explain why our catalysts are hydrophilic as opposed to TS-1. The new catalysts were highly active in cyclohexene epoxidation in both hydrophilic and hydrophobic environment, with excellent selectivity in particular in the latter, by far outperforming Ti-MCM-41 and, in particular, TS-1. In (hydrophilic) *n*-hexene epoxidation, however, the micro-mesophases failed completely while TS-1 exhibited high activity.

Acknowledgments

Financial support by the German Science foundation is gratefully acknowledged (Grant No. Gi 139/20). We are grateful for the TEM micrographs made by Dr. Zhiaofei Li. JAM and CEAK acknowledge the Flemish Government for long-term structural support via the centre of excellence (CECAT), the concerted research action (GOA), and Methusalem funding. AA acknowledges FWO for financial support.

References

- [1] J. Perez-Ramirez, C.H. Christensen, K. Egeblad, C.H. Christensen, J.C. Groen, *Chem. Soc. Rev.* 27 (2008) 2530–2542.
- [2] J. Cejka, S. Mintova, *Catal. Rev. Sci. Eng.* 49 (2007) 457–509.
- [3] C.J.H. Jacobsen, C. Madsen, J. Houzvicka, I. Schmidt, A. Carlsson, *J. Am. Chem. Soc.* 122 (2000) 7116–7117.
- [4] F.S. Xiao, L.F. Wang, C.Y. Yin, K.F. Lin, Y. Di, J.X. Li, D.S. Su, R. Schlögl, T. Yokoi, T. Tatsumi, *Angew. Chem. Int. Ed.* 45 (2006) 3090–3093.
- [5] M. Ogura, S.Y. Shinomiya, J. Tatenno, Y. Nara, M. Nomura, E. Kikuchi, M. Matsukata, *Appl. Catal. A* 219 (2001) 33–43.
- [6] J.A. Groen, L.A.A. Pfeffer, J.A. Moulijn, J. Perez-Ramirez, *Micropor. Mesopor. Mater.* 69 (2004) 29–34.
- [7] S. Mintova, *Colloid Czech Chem. Commun.* 68 (2003) 2032–2054.
- [8] D.T. On, S. Kaliaguine, *Angew. Chem. Int. Ed.* 40 (2001) 3248–3251.
- [9] M. Choi, D.G. Cho, R. Srivastava, C. Venkatesan, D.H. Choi, R. Ryoo, *Nat. Mater.* 5 (2006) 718–723.
- [10] Y. Liu, W.Z. Zhang, T.J. Pinnavaia, *J. Am. Chem. Soc.* 122 (2000) 8791.
- [11] Z.T. Zhang, Y. Han, F.S. Xiao, S.L. Qiu, L. Zhu, R.W. Wang, Y. Yu, Z. Zhang, B.S. Zou, Y.Q. Wang, H.P. Sun, D.Y. Zhao, Y. Wei, *J. Am. Chem. Soc.* 123 (2001) 5014.
- [12] X.Y. Yang, Y. Han, K.F. Lin, G. Tian, Y.F. Feng, X.J. Meng, Y. Di, Y.C. Du, Y.L. Zhang, F.S. Xiao, *Chem. Commun.* (2004) 2612.
- [13] Y. Liu, W.Z. Zhang, T.J. Pinnavaia, *Angew. Chem. Int. Ed.* 40 (2001) 1255–1258.
- [14] L. Zhu, F.-S. Xiao, Z. Zhang, Y. Sun, Y. Han, S. Qiu, *Catal. Today* 68 (2001) 209–216.
- [15] F.S. Xiao, Y. Han, Y. Yu, X.J. Meng, M. Yang, S. Wu, *J. Am. Chem. Soc.* 124 (2002) 888–889.
- [16] F.S. Xiao, Y. Han, X.J. Meng, Y. Yu, M. Yang, S. Wu, *Stud. Surf. Sci. Catal.* 146 (2003) 565–568.
- [17] X.J. Meng, D.F. Li, X.Y. Yang, Y. Yu, S. Wu, Y. Han, Q. Yang, D.Z. Jiang, F.S. Xiao, *J. Phys. Chem. B* 107 (2003) 8972–8980.
- [18] K.F. Lin, Z.H. Sun, L. Sen, D.Z. Jiang, F.S. Xiao, *Micropor. Mesopor. Mater.* 72 (2004) 193–201.
- [19] G.A. Eimer, I. Diaz, E. Sastre, S.G. Casuscelli, M.E. Crivello, E.R. Herrero, J. Perez-Pariante, *Appl. Catal. A* 343 (2008) 77–86.
- [20] P.A. Jacobs, H.K. Beyer, J. Valyon, *Zeolites* 1 (1981) 161–168.
- [21] S. Bordiga, P. Ugliengo, A. Damin, C. Lamberti, G. Spoto, A. Zecchina, G. Spano, R. Buzzoni, L. Dalloro, F. Rivetti, *Top. Catal.* 15 (2001) 43–52.

- [22] C.Z. Jin, G. Li, X.S. Wang, L.X. Zhao, L.P. Liu, H.I. Liu, Y. Liu, W.P. Zhang, X.W. Han, X.H. Bao, *Chem. Mater.* 19 (2007) 1664–1670.
- [23] M. Reichinger, H. Gies, M.W.E. van den Berg, W. Grünert, C. Kirschhock, *Stud. Surf. Sci. Catal.* 170 (2007) 276–281.
- [24] M. Reichinger, Ph.D. Thesis, Bochum, 2007.
- [25] A. Corma, M.T. Navarro, J. Perez-Pariente, *J. Chem. Soc., Chem. Commun.* (1994) 147.
- [26] F.W.H. Kampers, T.M.J. Maas, J. van Grondelle, D.C. Brinkgreve, D.C. Koningsberger, *Rev. Sci. Instrum.* 60 (1989) 2635–2638.
- [27] K.V. Klementiev, VIPER for Windows (Visual Processing in EXAFS Researches). <<http://www.desy.de/~klmn/viper.html>>.
- [28] Q. Huo, D.I. Margolese, G.D. Stucky, *Chem. Mater.* 8 (1996) 1147–1160.
- [29] R.W. Wang, L. Hu, B. Chu, L. Zhao, G.S. Zhu, S.L. Qiu, *Catal. Commun.* 6 (2005) 485–490.
- [30] F. Geobaldo, S. Bordiga, A. Zecchina, E. Giamello, G. Leofanti, G. Petrini, *Catal. Lett.* 16 (1992) 109–115.
- [31] S. Bordiga, F. Bonino, A. Damin, C. Lamberti, *J. Phys. Chem. B* 106 (2007) 9892–9905.
- [32] D. Lesthaeghe, P. Vansteenkiste, T. Verstraelen, A. Ghysels, C.E.A. Kirschhock, J.A. Martens, V. Van Speybroeck, M. Waroquier, *J. Phys. Chem. C* 112 (2008) 9186–9191.
- [33] C.E.A. Kirschhock, R. Ravishankar, F. Verspeurt, P.J. Grobet, P.A. Jacobs, J.A. Martens, *J. Phys. Chem. C* 103 (1999) 4965–4971.
- [34] F. Farges, G.E. Brown, J.J. Rehr, *Phys. Rev. B* 56 (1997) 1809–1819.
- [35] S. Bordiga, A. Damin, F. Bonino, A. Zecchina, G. Spano, F. Rivetti, V. Bolis, C. Prestipino, C. Lamberti, *J. Phys. Chem. B* 106 (2002) 9892–9905.
- [36] C.E.A. Kirschhock, S.P.B. Kremer, J. Vermant, G. Van Tendeloo, P.A. Jacobs, J.A. Martens, *Chem. Eur. J.* 11 (2005) 4306–4316.
- [37] S. Bals, K.J. Batenburg, D.D. Liang, O. Lebedev, G. Van Tendeloo, A. Aerts, J.A. Martens, C.E.A. Kirschhock, *J. Am. Chem. Soc.* 131 (2009) 4769–4773.